AEGIS: An adaptive ideal-magnetohydrodynamics shooting code for axisymmetric plasma stability

L.-J. Zheng *, M. Kotschenreuther

Institute for Fusion Studies, University of Texas at Austin, 1 University Station, C1500 Austin, TX 78712, United States

Abstract

A new linear ideal-magnetohydrodynamics stability code for axisymmetric plasmas, AEGIS, is described. The AEGIS code employs adaptive shooting in the radial direction and Fourier decomposition in the poloidal direction. The general solution is a linear combination of the independent solutions of the Euler–Lagrange equations solved by the adaptive shooting. A multiple-region matching technique is used to overcome the numerical difficulty associated with the stiff nature of the independent solutions. Benchmarks with other MHD codes show good agreement. Because it is adaptive, the AEGIS code has very good resolution near the singular surfaces of MHD modes. AEGIS has the additional advantage of allowing the investigation of modes with not only low mode numbers, but also intermediate to high mode numbers.
© 2005 Elsevier Inc. All rights reserved.

1. Introduction

Successful magnetic confinement of a toroidal fusion plasma relies on the magnetohydrodynamic (MHD) stability of the plasma. Due to the complexity of toroidal geometry, numerical computation of the MHD instability modes in toroidal plasmas is indispensable for interpreting experimental observations and designing new devices. During the last 30 years, several MHD stability codes have been developed, such as PEST, ERATO, GATO, DCON, NOVA, KINX, MISHKA, etc. [1–11].

---

* Corresponding author. Tel.: +1 512 471 3795; fax: +1 512 471 6715.
  E-mail address: lzheng@mail.utexas.edu (L.-J. Zheng).

The MHD eigenvalue-type codes – for example, PEST [1,2,6] and GATO [5] – usually employ the finite element method with a fixed grid for solving the radial eigenvalue problem. As is well known, the ideal MHD eigenvalue problem can be singular at mode rational surfaces in the case of marginal stability. To resolve this singular feature, an adaptive grid mesh in the radial dimension is desirable. The DCON code [7] employs an adaptive method; however, it uses the generalized Newcomb theorem [12] to determine stability of the internal modes and computes only the marginal stability of both internal and external MHD modes.

The current paper describes a newly developed adaptive eigenvalue shooting code for ideal MHD equations that can solve the finite frequency (or growth rate) eigenvalue problem. The finite frequency problem needs to be addressed in incorporating rotational and kinetic effects and in studying the Alfvén modes. Therefore, the numerical scheme presented in this article has the potential for being directly extended beyond low-frequency ideal MHD computations. The new code is named AEGIS (Adaptive EiGenfunction Independent Solution). The AEGIS code uses Fourier decomposition in the poloidal direction. To solve the radial eigenvalue problem, it constructs the general solution through a linear combination of the independent solutions of the Euler–Lagrange equations. The eigenvalue problem is then formulated by this general solution being fitted to the boundary conditions at the magnetic axis and the plasma-vacuum interface. This formulation is similar to that employed in the DCON code for marginal stability and in the ELITE code for high-mode-number MHD modes [13–15]. The difference from DCON is that AEGIS addresses modes with finite frequency or growth rate. The difference from ELITE is that AEGIS addresses both low- and intermediate-to-high-mode-number modes. To compute the eigenvalue problem with finite frequency (or growth rate), the modes at the singular layers must to be resolved. This poses a difficulty in applying the method based on decomposition in terms of the independent solutions. Although the MHD eigenmodes are well-behaved, the independent solutions are generally very stiff because near marginal stability the MHD modes are singular at the mode resonance surfaces, as well as at the magnetic axis. Hence, continuously shooting from the magnetic axis to the plasma edge usually fails to obtain accurately the independent solutions that extend across the whole plasma. The small solution of the Euler–Lagrange equation is often submerged in the numerical noise of the large solution. To resolve this difficulty, the AEGIS code employs a multiple-region matching technique. In this procedure, shooting in the radial dimension is performed in multiple regions, and then the independent solutions obtained in the individual regions are matched to each other. Note that the DCON code uses the Gaussian elimination technique to remove the large solution in order to resolve the numerical difficulty due to singularity at resonance surfaces. We find that our numerical scheme in AEGIS can effectively handle the ideal-MHD eigenvalue problem. It therefore opens the door for the extension to kinetic MHD computations, which in general need to deal with the MHD large solution.

The paper is arranged as follows: In Section 2, the equilibrium calculation is described. In Section 3, the numerical scheme for determining the independent solutions is detailed. The eigenvalue problem for determining the stability is then formulated with the use of these independent solutions. In Section 4, the numerical results and the benchmarks with the GATO code are described. In the last section, the results are discussed and conclusions are presented.

2. Equilibrium

In a toroidally symmetric configuration, the magnetic field $\vec{B}$ can be expressed as

$$\vec{B} = \chi'\nabla\phi \times \nabla\psi + g(\chi)\nabla\phi, \tag{1}$$

where ϕ is the axisymmetric toroidal angle, ψ labels the magnetic surface, $\chi(\psi)$ denotes the poloidal magnetic flux, $g(\chi)$ is the poloidal current flux and a prime denotes a derivative with respect to ψ. An overhead arrow is used to indicate vectors in configuration space. The poloidal flux χ is governed by the Grad-Shafranov equation, with the pressure profile $P(\chi)$ and poloidal current flux $g(\chi)$ to be specified. The

Grad-Shafranov equation usually needs to be solved numerically by means of an equilibrium code, for example, TOQ [16]. The numerical equilibrium data computed by an equilibrium code become the input to AEGIS. The data required by AEGIS are the profile functions for poloidal magnetic flux $\chi(\psi)$, pressure $P(\psi)$ and poloidal current flux $g(\psi)$ and the flux coordinates $X(\psi, \theta)$ and $Z(\psi, \theta)$ at the grid points. Here, X and Z are Cartesian coordinates in the $\phi = \mathrm{const}$ plane and θ is the poloidal coordinate (which, in the case of TOQ, is the equal-arc-length poloidal coordinate).

As with most MHD codes, AEGIS performs re-gridding, both for the radial coordinate and the poloidal angle. The re-gridding relies on spline interpolations of the equilibrium data. As proposed in the PEST1 code, [1] the coordinate splines are established on a generalized polar coordinate system. During the re-gridding, there is a choice with respect to various coordinate systems, such as equal-arc-length coordinates, the PEST coordinate system [1] and the Hamada [17] coordinate system. The equal-arc-length and PEST coordinate systems are shown in Figs. 1 and 2, respectively.

As described in Section 1, the independent solutions of the linear Euler–Lagrange equations are obtained by shooting in multiple radial regions. As shown in Fig. 3, the radial grids are grouped region by region. Each region usually contains a single mode resonance surface. Therefore, the number of regions depends on the toroidal mode number n and the safety factor q profile. Additional regions can be added near the magnetic axis, depending on how stiff the shooting is in this area.
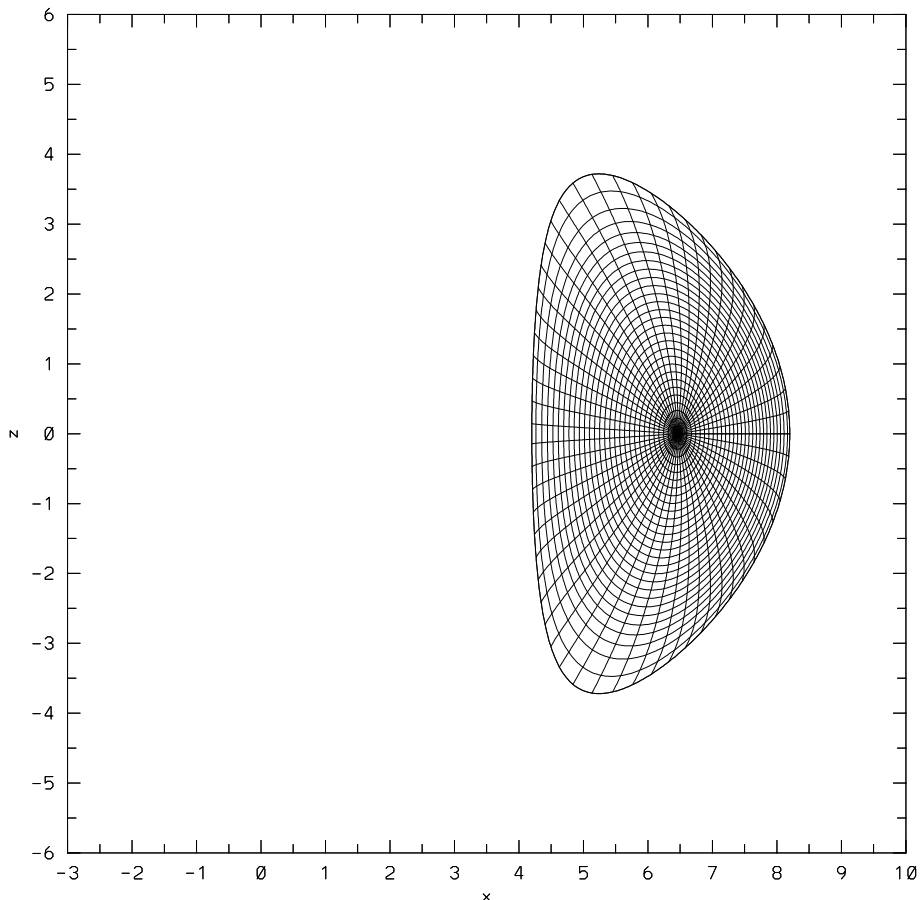

Fig. 1. The equal arc length coordinate system as read from the equilibrium code TOQ. The figure takes the ITER-like cross-section parameters: elongation $\kappa = 1.8$ and triangularity $\delta = 0.5$.
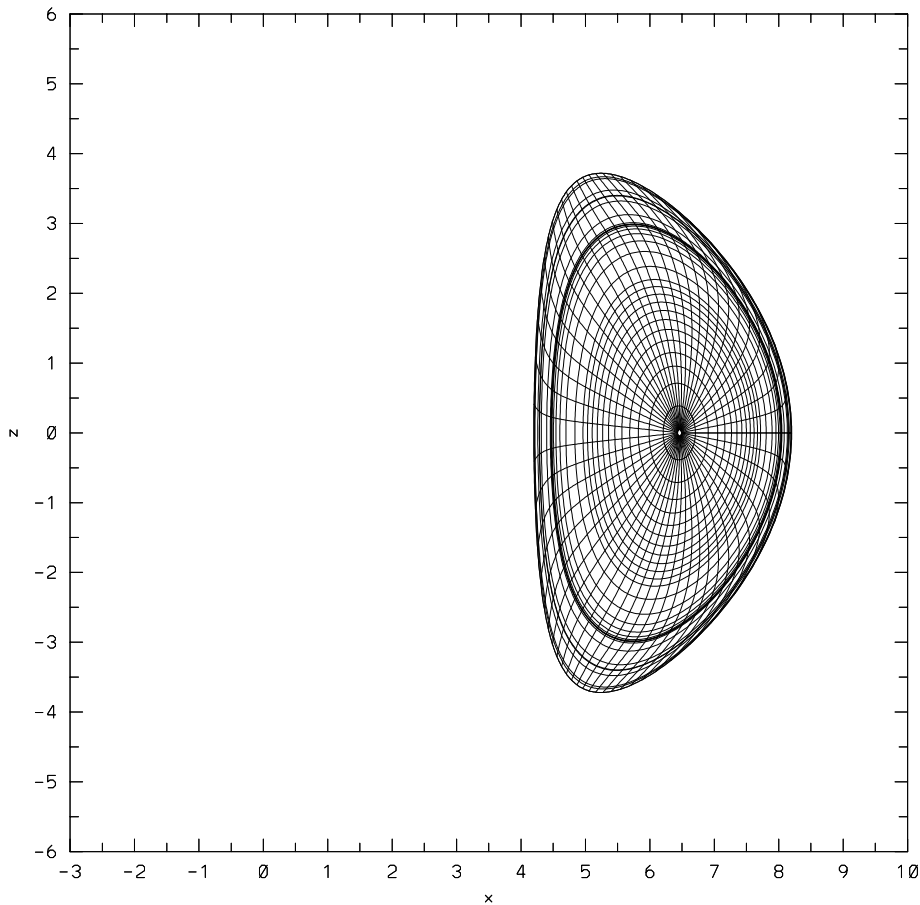
Fig. 2. The Fig. 1 equilibrium is regrided into the PEST coordinate system. Denser grids are placed at the MHD mode resonance surfaces.

As shown in Fig. 3, denser grids can be placed near the resonance surfaces, according to a polynomial-type grid density distribution that can be selected. The GATO code uses a similar arrangement. In the AE-GIS adaptive scheme, however, the shooting is not based on the specified radial grid. Instead, the grid is merely used to impose the maximum step size in the adaptive shooting at various radii.

As will be described in the next section in more detail, the equilibrium quantities required for solving the linear Euler–Lagrange equations are Fourier decomposed in the poloidal angle to form various equilibrium matrices. In the equilibrium calculation, each element of the matrices is first computed at the radial grids and then made to become a radially continuous function by spline interpolation.

3. Stability

Here we consider only a system in which a plasma torus is surrounded by a perfectly conducting wall. The investigation of stability involves the minimization of the field and plasma energies, both in the plasma and the vacuum regions. The minimization is realized through the solution of the corresponding Euler–Lagrange equations with proper boundary conditions.
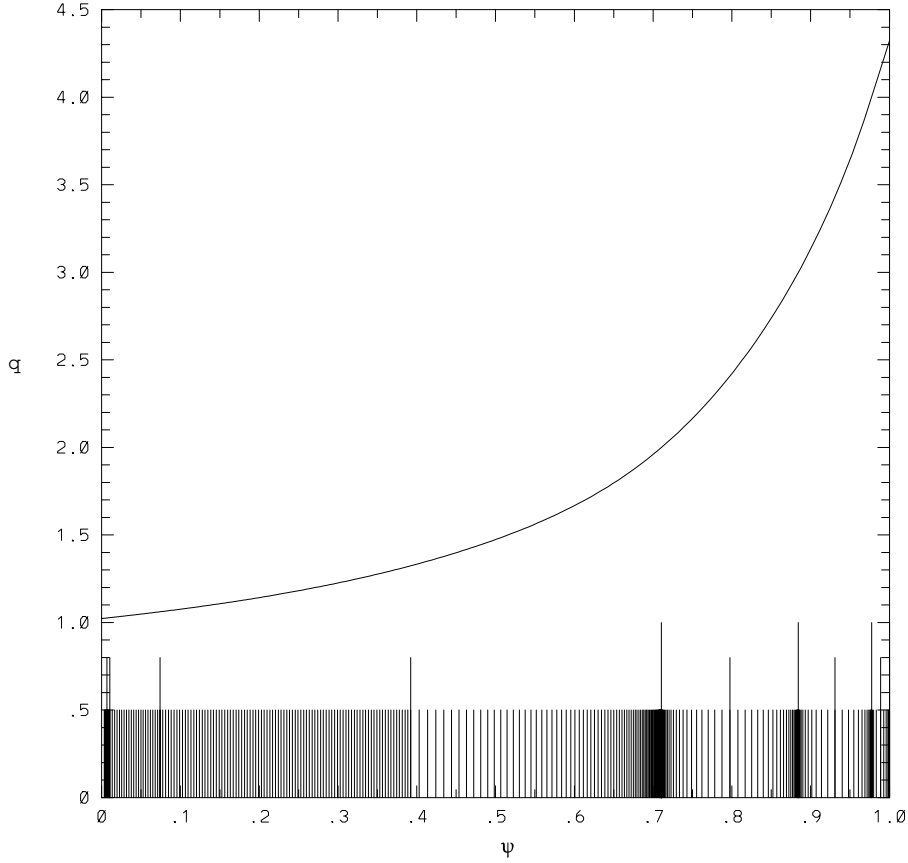
Fig. 3. An example of the shooting region setup together with the q profile. The highest vertical lines shows the mode resonance surfaces (for $n = 1$ modes), the medium high vertical lines indicate the region separation surfaces and the short vertical lines specify the radial grids, which imposes the maximum step size in the shooting.

3.1. Plasma region

Although AEGIS is coded so as to be used with three coordinate systems – i.e., PEST, equal-arc-length and Hamada coordinates – here, for simplicity, we describe only the procedure with PEST coordinates (ψ, θ, ϕ). The Jacobian for PEST coordinates is given as follows [1]:

$$\mathscr{J} = \frac{1}{\nabla\psi \times \nabla\theta \cdot \nabla\phi} = \frac{vX^2}{2\pi R} = \frac{\chi' qX^2}{g}, \tag{2}$$

where R is the major radius of the magnetic axis and v is a constant.

The plasma potential energy and kinetic energy can be expressed, respectively, as follows:

$$\delta W_{\mathrm{p}} = \frac{1}{2\mu_0} \int \mathrm{d}\tau \left\{ \left| \vec{Q} + \mu_0 \frac{(\vec{\xi} \cdot \nabla\psi)\vec{J} \times \nabla\psi}{|\nabla\psi|^2} \right|^2 - 2U|\vec{\xi} \cdot \nabla\psi|^2 \right\}, \tag{3}$$

$$\delta W_{\mathrm{k}} = -\frac{1}{2} \int \mathrm{d}\tau \rho \gamma^2 |\vec{\xi}_\perp|^2, \tag{4}$$

where μ_0 represents the permeability of free space, $\vec{\xi}$ is the magnetic field line displacement vector, $\vec{Q} = \nabla \times \vec{\xi} \times \vec{B}$, $\vec{J}$ is the equilibrium current density vector:

$$2U = 2\mu_0 P' \kappa_\psi + \frac{\sigma^2 B^2}{|\nabla\psi|^2} + \frac{\chi' g}{X^2} \frac{\partial}{\partial\theta}\left(\frac{\sigma\nabla\psi \cdot \nabla\theta}{|\nabla\psi|^2}\right) + \chi' \frac{\sigma q' g}{qX^2},$$

$$\sigma = \frac{\mu_0 \vec{J} \cdot \vec{B}}{B^2} = -\frac{\mu_0 p' g}{B^2 \chi'} - \frac{g'}{\chi'},$$

$$\kappa_\psi = \frac{\mu_0 P'}{B^2} + \frac{1}{2B^2}\frac{\partial B^2}{\partial\psi} + \frac{\chi'^2}{2B^4}\frac{\nabla\psi \cdot \nabla\theta}{X^2}\frac{\partial B^2}{\partial\theta},$$

where γ is the growth rate, ρ denotes the density and $d\tau$ represents the differential volume element. Plasma compressibility is neglected here, since that it contributes only to an apparent mass effect and does not affect the MHD marginal stability criterion.

Since the effect of compressibility is excluded, the parallel component of $\vec{\xi}$ can be ignored. Therefore, one can decompose $\vec{\xi}$ as follows:

$$\vec{\xi} = \xi^\psi \chi' \frac{\vec{B} \times \vec{s}}{B^2} + i \xi^s \chi' \frac{\vec{B} \times \nabla\psi}{B^2}, \tag{5}$$

where $\vec{s} = \nabla\phi - q\nabla\theta$. We represent ξ^ψ as follows:

$$\xi^s = \frac{1}{n}\frac{\partial\xi^\psi}{\partial\psi} + \delta.$$

The ballooning stream function type of representation in Eq. (5) simplifies the matrices to be constructed, due to the minimization with respect to the effect of the compressional Alfvén mode. The $n = 0$ mode is excluded from consideration in the current version of the AEGIS code. Furthermore, Fourier decomposition is performed for the linear perturbations:

$$\xi^\psi = \sum_{m=m_{\min}}^{m_{\max}} \xi_m^\psi \exp\{i(m\theta - n\phi)\}, \tag{6}$$

where $m_{\max}$ and $m_{\min}$ are, respectively, the maximum and minimum sideband poloidal mode numbers to be considered.

Inserting the expressions in Eqs. (5) and (6) into Eqs. (3) and (4), the potential and kinetic energies can be formulated in terms of the matrices in Fourier space as follows:

$$2\mu_0(\delta W_{\mathrm{p}} + \delta W_{\mathrm{k}}) = \int d\psi \left(\begin{array}{ccc} \boldsymbol{\xi}^{\psi\dagger} & \boldsymbol{\xi}^{\psi'\dagger} & \boldsymbol{\delta}^\dagger \end{array}\right) \begin{pmatrix} \mathscr{A} & \mathscr{P} & \mathscr{R} \\ \mathscr{P}^\dagger & \mathscr{B} & \mathscr{Q} \\ \mathscr{R}^\dagger & \mathscr{Q}^\dagger & \mathscr{C} \end{pmatrix} \begin{pmatrix} \boldsymbol{\xi}^\psi \\ \boldsymbol{\xi}^{\psi'} \\ \boldsymbol{\delta} \end{pmatrix}. \tag{7}$$

Here, a dagger denotes the conjugate of a matrix and boldface denotes a vector in Fourier space, i.e., a single-column matrix, for example,

$$\boldsymbol{\xi}^\psi = \begin{pmatrix} \xi_1^\psi \\ \vdots \\ \xi_M^\psi \end{pmatrix}, \qquad \boldsymbol{\delta} = \begin{pmatrix} \delta_1 \\ \vdots \\ \delta_M \end{pmatrix},$$

where the poloidal Fourier components are numbered from $m_{\min}$ to $m_{\max}$ and the total number of Fourier components under consideration is by $M = m_{\max} - m_{\min} + 1$. The equilibrium matrices are given as follows:

$$\begin{pmatrix} \mathscr{A} & \mathscr{P} & \mathscr{R} \\ \mathscr{P}^\dagger & \mathscr{B} & \mathscr{Q} \\ \mathscr{R}^\dagger & \mathscr{Q}^\dagger & \mathscr{C} \end{pmatrix} = \begin{pmatrix} \mathscr{A}_p & \mathscr{P}_p & \mathscr{R}_p \\ \mathscr{P}_p^\dagger & \mathscr{B}_p & \mathscr{Q}_p \\ \mathscr{R}_p^\dagger & \mathscr{Q}_p^\dagger & \mathscr{C}_p \end{pmatrix} + \rho\gamma^2 \begin{pmatrix} \Gamma & \Sigma & \Upsilon \\ \Sigma^\dagger & \Xi & \Lambda \\ \Upsilon^\dagger & \Lambda^\dagger & \Pi \end{pmatrix}.$$

Here, $\mathscr{A}, \mathscr{B}$, etc., are $M \times M$ matrices, defined as follows:

$$\mathscr{A}_p = \frac{\chi'^3 q}{g} \mathscr{K}_\parallel \langle |\nabla\theta|^2 \rangle \mathscr{K}_\parallel + \frac{\chi'\chi''^2 q}{g} \langle |\nabla\psi|^2 \rangle + \frac{g(q\chi')'^2}{\chi' q} \mathscr{I} + \mu_0 p' \frac{q\chi''}{g} \langle X^2 \rangle$$
$$+ \mu_0 P' \frac{\chi' q}{g} \left\langle \frac{\partial X^2}{\partial \psi} \right\rangle - g' q' \chi' \mathscr{I} - \mathrm{i} \frac{\chi'^2 \chi'' q}{g} (\langle \nabla\psi \cdot \nabla\theta \rangle \mathscr{M} - \mathscr{M} \langle \nabla\psi \cdot \nabla\theta \rangle),$$

$$\mathscr{B}_p = \frac{\chi' g}{n^2 q} \mathscr{K}_\parallel \mathscr{K}_\parallel,$$

$$\mathscr{C}_p = \frac{\chi' g}{q} \mathscr{M} \mathscr{M} + \frac{n^2 \chi'^3 q}{g} \langle |\nabla\psi|^2 \rangle,$$

$$\mathscr{P}_p = 0,$$

$$\mathscr{Q}_p = \frac{\chi' g}{nq} \mathscr{M} \mathscr{K}_\parallel,$$

$$\mathscr{R}_p = \mathrm{i} \frac{n\chi'^3 q}{g} \langle \nabla\psi \cdot \nabla\theta \rangle \mathscr{K}_\parallel - \mu_0 n P' \frac{\chi' q}{g} \langle X^2 \rangle - \frac{n\chi'^2 \chi'' q}{g} \langle |\nabla\psi|^2 \rangle - n\chi' q g' \mathscr{I},$$

$$\Gamma = \frac{\chi'^3 q}{g} \left(\left\langle \frac{1}{B^2} \right\rangle + q^2 \left\langle \frac{X^2 |\nabla\theta|^2}{B^2} \right\rangle \right),$$

$$\Xi = \frac{\chi'^3 q}{n^2 g} \left\langle \frac{X^2 |\nabla\psi|^2}{B^2} \right\rangle,$$

$$\Pi = n^2 \Xi,$$

$$\Sigma = -\mathrm{i} \frac{\chi'^3 q^2}{ng} \left\langle \frac{X^2 \nabla\psi \cdot \nabla\theta}{B^2} \right\rangle,$$

$$\Lambda = n\Xi,$$

$$\Upsilon = n\Sigma.$$

An angle bracket $\langle \cdots \rangle$ represents the associated Fourier matrix, whose elements are defined as follows:

$$\langle \cdots \rangle_{mm'} = \frac{1}{2\pi} \int_{-\pi}^{\pi} \mathrm{d}\theta (\cdots) \exp\{\mathrm{i}(m' - m)\theta\},$$

and $\mathscr{K}_{\parallel mm'} = (m - nq)\mathscr{I}_{mm'}$, $\mathscr{M}_{mm'} = m\mathscr{I}_{mm'}$, and $\mathscr{I}_{mm'} = 1$ for $m = m'$, otherwise, $\mathscr{I}_{mm'} = 0$, where $m, m' = 1, 2, \ldots, M$.

To suppress the compressional Alfvén contribution, the total plasma energy in Eq. (7) is varied with respect to $\boldsymbol{\delta}^\dagger$, yielding

$$\mathscr{R}^\dagger \boldsymbol{\xi}^\psi + \mathscr{Q}^\dagger \boldsymbol{\xi}'^\psi + \mathscr{C} \boldsymbol{\delta} = 0. \tag{8}$$

This is an algebraic equation and can be solved:

$$\boldsymbol{\delta} = \left(-\mathscr{C}^{-1} \mathscr{R}^\dagger \quad -\mathscr{C}^{-1} \mathscr{Q}^\dagger \right) \begin{pmatrix} \boldsymbol{\xi}^\psi \\ \boldsymbol{\xi}'^\psi \end{pmatrix}. \tag{9}$$

Inserting Eq. (9) back into Eq. (7), we reduce the plasma energy integral to

$$2\mu_0(\delta W_{\mathrm{p}} + \delta W_{\mathrm{k}}) = \int \mathrm{d}\psi \big(\boldsymbol{\xi}^{\psi\prime\dagger} \quad \boldsymbol{\xi}^{\psi\dagger} \big) \begin{pmatrix} \mathscr{F} & \mathscr{K} \\ \mathscr{K}^\dagger & \mathscr{G} \end{pmatrix} \begin{pmatrix} \boldsymbol{\xi}^{\psi\prime} \\ \boldsymbol{\xi}^{\psi} \end{pmatrix}, \tag{10}$$

where

$$\mathscr{F} = \mathscr{B} - \mathscr{Q}\mathscr{C}^{-1}\mathscr{Q}^\dagger,$$
$$\mathscr{K}^\dagger = \mathscr{P} - \mathscr{R}\mathscr{C}^{-1}\mathscr{Q}^\dagger,$$
$$\mathscr{G} = \mathscr{A} - \mathscr{R}\mathscr{C}^{-1}\mathscr{R}^\dagger.$$

We can further minimize the plasma energy by it varying Eq. (10) with respect to $\boldsymbol{\xi}^{\psi\dagger}$, which gives rise to the set of Euler–Lagrange equations

$$\big(\mathscr{F}\boldsymbol{\xi}^{\psi\prime} + \mathscr{K}\boldsymbol{\xi}^{\psi}\big)' - \mathscr{K}^\dagger\boldsymbol{\xi}^{\psi\prime} - \mathscr{G}\boldsymbol{\xi}^{\psi} = 0.$$

As in the DCON code, this set of equations can be reformulated to a set of first-order differential equations

$$\mathbf{u}' = \mathscr{L}_{\mathrm{p}}\mathbf{u}, \tag{11}$$

where

$$\mathbf{u} \equiv \begin{pmatrix} \mathbf{u}_1 \\ \mathbf{u}_2 \end{pmatrix} = \begin{pmatrix} \boldsymbol{\xi}^{\psi} \\ \mathscr{F}\boldsymbol{\xi}^{\psi\prime} + \mathscr{K}\boldsymbol{\xi}^{\psi} \end{pmatrix},$$
$$\mathscr{L}_{\mathrm{p}} = \begin{pmatrix} -\mathscr{F}^{-1}\mathscr{K} & \mathscr{F}^{-1} \\ \mathscr{G} - \mathscr{K}^\dagger\mathscr{F}^{-1}\mathscr{K} & \mathscr{K}^\dagger\mathscr{F}^{-1} \end{pmatrix}.$$

Using integration by parts, one can show that for the solution of the set of Euler–Lagrange Eq. (11), the energy integral in Eq. (10) only contributes at the plasma–vacuum interface ψ_a

$$2\mu_0(\delta W_{\mathrm{p}} + \delta W_{\mathrm{k}}) = \mathbf{u}_1^\dagger\mathbf{u}_2\big|_{\psi=\psi_a}. \tag{12}$$

To solve Eq. (11), we first seek the complete set of independent solutions. We then use these independent solutions to construct the eigensolution that satisfies the boundary conditions. The adaptive-mesh shooting method is used to obtain the independent solutions. On account of the stiff nature of the equations caused by the singular mode surfaces and the magnetic axis, we find that shooting continuously from the magnetic axis to the plasma edge usually gives rise to solutions that are quite numerically polluted. Even if this difficulty could be coped with by a high-accuracy shooting routine, the resulting eigenmatrix can still be ill-conditioned. To curb these problems, we employ a multiple-region shooting scheme. In this scheme, the entire region from the plasma's magnetic axis to the plasma edge is divided into L regions, separated by $\psi_0, \psi_1, \ldots, \psi_L \equiv \psi_a$, where ψ_0 is at the vicinity of the magnetic axis. Each region usually contains only a single mode resonance surface, except near the magnetic axis where more divided regions are usually placed.

Note that Eq. (11) is a set of $2M$ first-order differential equations. Therefore, in general there are $2M$ independent solutions for Eq. (11). In the first region, however, M boundary conditions can be imposed at the magnetic axis and therefore the total number of independent solutions in the first region is reduced to M. We define $M_l = 2M$ for $l > 1$ and $M_1 = M$. The kth independent solution in the lth region is denoted by ${}^l\mathbf{u}^k \equiv \begin{pmatrix} {}^l\mathbf{u}_1^k \\ {}^l\mathbf{u}_2^k \end{pmatrix}$, where $k = 1, 2, \ldots, M_l$ and $l = 1, 2, \ldots, L$. The independent solutions are obtained by shooting with independent initial conditions.

The boundary conditions at the magnetic axis can be approximated by the cylinder solutions [7,10]

$$\xi_m^\psi \propto r^m, \tag{13}$$

where the average minor radius $r \propto \sqrt{V}$, with V the volume inside ψ_0. Here, we note that ψ_0 is adjusted such that it is not a mode rational surface. In the first region the kth independent solution ${}^1\mathbf{u}_1^k$ can be initiated as

$${}^1u_{1m}^k(\psi_0) = \mathscr{I}_{mk}, \quad \text{for } m,k = 1,2,\ldots,M \tag{14}$$

and subsequently ${}^1u_{2m}^k$ can be obtained by the use of Eq. (13) for $\xi_m^{\psi\prime}/\xi_m^\psi$. In the remaining regions the initial conditions are simply

$${}^lu_m^k(\psi_{l-1}) = \mathscr{I}_{mk}, \quad \text{for } m,k = 1,2,\ldots,2M \text{ and } l = 2,\ldots,L. \tag{15}$$

From the theory of differential equations, the general solution in the lth region can be represented as a linear combination of the independent solutions

$${}^l\mathbf{u} = \sum_{k=1}^{M_l} {}^l\mathbf{u}^{kl}c_k = {}^l\mathscr{U}^{2M \times M_l l}\mathbf{c}, \quad \text{for } l = 2,\ldots,L, \tag{16}$$

where ${}^lc_k$ are constants to be determined by the boundary conditions and matching conditions, with

$${}^l\mathbf{c} = \begin{pmatrix} {}^lc_1 \\ \vdots \\ {}^lc_M \end{pmatrix}$$

being the matrix representation of these constants. The independent solutions in the lth shooting region are used to construct the independent solution matrices ${}^l\mathscr{U}^{2M \times M_l} \equiv \begin{pmatrix} {}^l\mathscr{U}_1^{M \times M_l} \\ {}^l\mathscr{U}_2^{M \times M_l} \end{pmatrix} = \{{}^l\mathbf{u}^1, {}^l\mathbf{u}^2, \ldots, {}^l\mathbf{u}^{M_l}\}$. The rank of the matrix is explicitly specified by the right superscript, which indicates the number of rows times the number of columns.

3.2. Vacuum region

The vacuum solution can usually be solved by the Green's function method [18]. The finite element method can be used to calculate the vacuum energy [19]. Here, we describe an alternative method based on the shooting method for the independent solutions. Our numerical experience is that this method is considerably faster than the Green's function method. However, this new method applies only to the vacuum region between the plasma and the surrounding wall. Shooting from the plasma or the wall to infinity is impractical. Although this shooting method can be coupled to various types of walls, here we consider only a perfectly conducting wall, for which we will benchmark the results with GATO, as described in the next section.

To use the shooting method, we first need to set up grids in the vacuum region between the plasma and the first wall, so that the metric parameters can be computed. Various types of grids can be used for this purpose. Fig. 4 shows equal-distance grids both radially and poloidally in the conformal wall case. We introduce the variables ψ and θ for labeling the radial and poloidal grids, respectively. In this grid system, therefore, we have the coordinates $X(\psi, \theta)$ and $Z(\psi, \theta)$. The toroidal axisymmetric angle ϕ can be chosen as the third coordinate. In this grid system one can then compute the Jacobian $\mathscr{J} = 1/\nabla\psi \times \nabla\theta \cdot \nabla\phi$ and the metric parameters $|\nabla\psi|^2$, $\nabla\psi \cdot \nabla\theta$, $|\nabla\theta|^2$ and $|\nabla\phi|^2$.
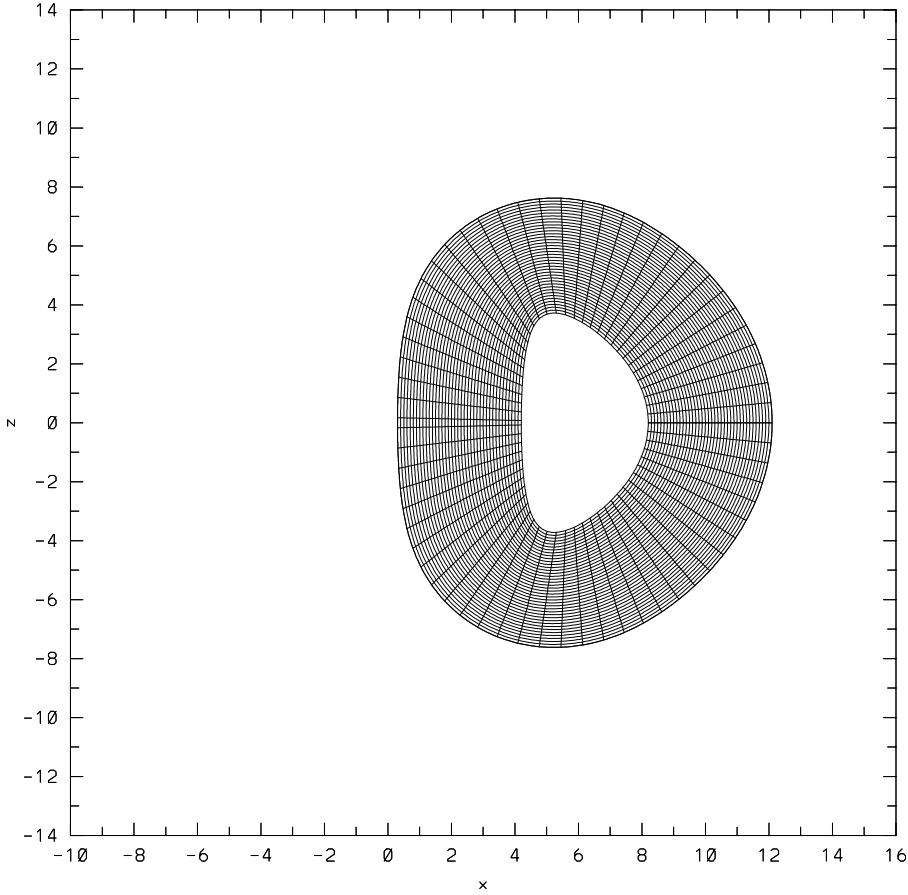
Fig. 4. The vacuum grid setup with a conformal wall.

The vacuum energy can be expressed in this coordinate system as follows:

$$
2\mu_0\delta W_{\rm v} = \int {\rm d}\tau|\nabla\varphi|^2 = \int {\rm d}\psi\, {\rm d}\theta\Bigg\{\frac{\partial\varphi^\dagger}{\partial\psi}\mathscr{J}|\nabla\psi|^2\frac{\partial\varphi}{\partial\psi} + \frac{\partial\varphi^\dagger}{\partial\theta}\mathscr{J}\nabla\psi\cdot\nabla\theta\frac{\partial\varphi}{\partial\psi} + \frac{\partial\varphi^\dagger}{\partial\psi}\mathscr{J}\nabla\psi\cdot\nabla\theta\frac{\partial\varphi}{\partial\theta}
$$
$$
+ \frac{\partial\varphi^\dagger}{\partial\theta}\mathscr{J}|\nabla\theta|^2\frac{\partial\varphi}{\partial\theta} + \varphi^\dagger n^2\mathscr{J}|\nabla\phi|^2\varphi\Bigg\}.
$$

Introducing poloidal Fourier decomposition, we can reduce the expression for the vacuum energy integral to

$$
2\mu_0\delta W_{\rm v} = \int {\rm d}\psi\begin{pmatrix}\frac{\partial\boldsymbol{\varphi}^\dagger}{\partial\psi} & \boldsymbol{\varphi}^\dagger\end{pmatrix}\begin{pmatrix}\mathscr{F}_{\rm v} & \mathscr{K}_{\rm v} \\ \mathscr{K}_{\rm v}^\dagger & \mathscr{G}_{\rm v}\end{pmatrix}\begin{pmatrix}\frac{\partial\boldsymbol{\varphi}}{\partial\psi} \\ \boldsymbol{\varphi}\end{pmatrix}, \tag{17}
$$

where $\mathscr{F}_{\rm v} = \langle\mathscr{J}|\nabla\psi|^2\rangle$, $\mathscr{K}_{\rm v} = {\rm i}\langle\mathscr{J}\nabla\psi\cdot\nabla\theta\rangle\mathcal{M}$, and $\mathscr{G}_{\rm v} = \mathcal{M}\langle\mathscr{J}|\nabla\theta|^2\rangle\mathcal{M} + n^2\langle\mathscr{J}/X^2\rangle$. Similar to the treatment in the plasma region, variation of Eq. (17) with respect to $\boldsymbol{\varphi}^\dagger$ yields the following set of Euler–Lagrange equations:

$$
\mathbf{u}_{\rm v}' = \mathscr{L}_{\rm v}\mathbf{u}_{\rm v}, \tag{18}
$$

where

$$\mathbf{u}_v \equiv \begin{pmatrix} \mathbf{u}_{v1} \\ \mathbf{u}_{v2} \end{pmatrix} = \begin{pmatrix} \boldsymbol{\varphi} \\ \mathscr{F}_v \boldsymbol{\varphi}' + \mathscr{K}_v \boldsymbol{\varphi} \end{pmatrix},$$

$$\mathscr{L}_v = \begin{pmatrix} -\mathscr{F}_v^{-1} \mathscr{K}_v & \mathscr{F}_v^{-1} \\ \mathscr{G}_v - \mathscr{K}_v^\dagger \mathscr{F}_v^{-1} \mathscr{K}_v & \mathscr{K}_v^\dagger \mathscr{F}_v^{-1} \end{pmatrix}.$$

Here, the subscript v is introduced to denote quantities in the vacuum region. For the solutions of the set of Euler–Lagrange Eq. (18), the energy integral in Eq. (17) can be reduced to a contribution at the plasma–vacuum interface:

$$2\mu_0 \delta W_v = -\mathbf{u}_{v1}^\dagger \mathbf{u}_{v2}\big|_{\psi=\psi_a}, \tag{19}$$

where the boundary condition at a perfectly conducting wall has been used. At the position of the perfectly conducting wall ψ_b, the normal magnetic field should vanish $\vec{B} \cdot \nabla \psi = 0$. Noting that $u_{v2m} \propto \delta\vec{B} \cdot \nabla\psi$, one has

$$\mathbf{u}_{v2}(\psi_b) = 0. \tag{20}$$

Eq. (20) can be used as the initial conditions for shooting from the wall to the plasma. Hence, there are only M independent solutions $\mathbf{u}_v^k$ ($k = 1, \ldots, M$) for Eq. (18). These M independent solutions can be obtained by means of the shooting method, with the following M set of initial conditions at the vacuum-wall interface:

$$u_{vm}^k(\psi_b) = \mathscr{I}_{mk}, \quad \text{for } m = 1, \ldots, 2M \text{ and } k = 1, \ldots, M. \tag{21}$$

Similar to the case in the plasma, the general solution in the vacuum region can be represented as a linear combination of the independent solutions:

$$\mathbf{u}_v = \sum_{k=1}^M \mathbf{u}_v^k c_{vk} = \mathscr{U}_v^{2M \times M} \mathbf{c}_v, \tag{22}$$

where c_{vk} are constants to be determined. The independent solutions are used to construct the independent solution matrices $\mathscr{U}_v^{2M \times M} \equiv \begin{pmatrix} \mathscr{U}_{v1}^{M \times M} \\ \mathscr{U}_{v2}^{M \times M} \end{pmatrix} = \{\mathbf{u}_v^1, \mathbf{u}_v^2, \ldots, \mathbf{u}_v^M\}$.

3.3. Eigenvalue problem

With the numerical shooting procedures described in the preceding two subsections, one can numerically obtain the general solutions both in the plasma region and in the vacuum region. The boundary conditions at the magnetic axis and at the perfectly conducting wall are imposed on these solutions. In this section, we describe the procedure to match the solutions between the shooting regions in the plasma and at the plasma–vacuum interface in order to derive the eigenmode equation. The matching procedure consists of two steps in order to distinguish the internal unstable modes from the external ones.

In the first matching step, the independent solutions in various shooting regions in the plasma are matched to each other, requiring $\mathbf{u}_p$ to be continuous, where the subscript p denotes quantities in the plasma region. It is apparent that, after internal matching, only M overall independent solutions are left, which are continuous in the plasma. We denote these M overall independent solutions as $\mathbf{u}_p^k = \begin{pmatrix} \mathbf{u}_{p1}^k \\ \mathbf{u}_{p2}^k \end{pmatrix}$ with $k = 1, 2, \ldots, M$ and further require that

$$u_{p1m}^k = \mathscr{I}_{mk}, \quad \text{for } m, k = 1, 2, \ldots, M. \tag{23}$$

The matching between the regions and the requirement in Eq. (23) can be jointly expressed by means of the following matrix equation:

$$\mathscr{Y}\begin{pmatrix} {}^{1}\mathscr{C}^{M \times M} \\ {}^{2}\mathscr{C}^{2M \times M} \\ \vdots \\ {}^{L-1}\mathscr{C}^{2M \times M} \\ {}^{L}\mathscr{C}^{2M \times M} \end{pmatrix} = \begin{pmatrix} 0^{2M \times M} \\ 0^{2M \times M} \\ \vdots \\ 0^{2M \times M} \\ \mathscr{I}^{M \times M} \end{pmatrix}, \tag{24}$$

with the matrices ${}^{l}\mathscr{C}^{M_{l} \times M} = \{{}^{l}\mathbf{c}^{1}, \dots, {}^{l}\mathbf{c}^{M}\}$, for which the kth column (${}^{l}\mathbf{c}^{k}$) corresponds to the kth component of the boundary conditions given in Eq. (23) and

$$\mathscr{Y}(\gamma) = \begin{pmatrix} {}^{1}\mathscr{U}^{2M \times M} & -\mathscr{I}^{2M \times 2M} & 0^{2M \times 2M} & \cdots & 0^{2M \times 2M} \\ 0^{2M \times M} & {}^{2}\mathscr{U}^{2M \times 2M} & -\mathscr{I}^{2M \times 2M} & \cdots & 0^{2M \times 2M} \\ \vdots & \vdots & \vdots & \vdots & \vdots \\ 0^{2M \times M} & \cdots & 0^{2M \times 2M} & {}^{L-1}\mathscr{U}^{2M \times 2M} & -\mathscr{I}^{2M \times 2M} \\ 0^{M \times M} & \cdots & 0^{M \times 2M} & 0^{M \times 2M} & {}^{L}\mathscr{U}_{1}^{M \times 2M} \end{pmatrix}.$$

Here, ${}^{l}\mathscr{U}^{2M \times M_{l}}$ ($l = 1, \dots, L-1$) and ${}^{L}\mathscr{U}_{1}^{M \times 2M}$ are evaluated at the upper (i.e., large major radius) end, ψ_{l}, of the respective region in the plasma.

There are two cases to consider. In the case when $\det \mathscr{Y}(\gamma) = 0$ for a given growth rate γ, the matrix $\mathscr{Y}$ is not invertible and therefore Eq. (24) has no trivial solution. In this case, however, the equation

$$\mathscr{Y}\begin{pmatrix} {}^{1}\mathbf{c} \\ \vdots \\ {}^{L}\mathbf{c} \end{pmatrix} = 0, \tag{25}$$

has a nontrivial solution instead. This means that there exists a solution that is continuous in the plasma (specified by the first $L-1$ rows of Eq. (25)) and that satisfies $\xi_{m}^{\psi}(\psi_{a}) = 0$ for all m (specified by the last row of Eq. (25)). Physically, this implies the existence of the internal mode.

In the case when $\det \mathscr{Y} \neq 0$, one can solve Eq. (24) for ${}^{l}\mathscr{C}^{M_{l} \times M}$. One can then construct a new set of M independent solutions

$$\mathscr{U}_{p}^{2M \times M}(\psi) = {}^{l}\mathscr{U}^{2M \times M_{l}l}\mathscr{C}^{M_{l} \times M}, \quad \text{for } \psi_{l-1} \leqslant \psi \leqslant \psi_{l}. \tag{26}$$

Here, we have $\mathscr{U}_{p}^{2M \times M} \equiv \begin{pmatrix} \mathscr{U}_{p1}^{M \times M} \\ \mathscr{U}_{p2}^{M \times M} \end{pmatrix} = \{\mathbf{u}_{p}^{1}, \mathbf{u}_{p}^{2}, \dots, \mathbf{u}_{p}^{M}\}$, for which each column represents an independent solution of the set of Euler–Lagrange Eq. (11). This set of independent solutions is continuous in the plasma (specified by the first $L-1$ rows of Eq. (24)) and satisfies the boundary condition (specified by the last row of Eq. (24))

$$\mathscr{U}_{p1}^{M \times M}(\psi_{a}) = \mathscr{I}. \tag{27}$$

The general solution ($\mathbf{u}_{p}$) of the Euler–Lagrange equations in the plasma region can therefore be constructed in terms of this new set of independent solutions:

$$\mathbf{u}_{p} = \mathscr{U}_{p}^{2M \times M}\mathbf{c}_{p}, \tag{28}$$

where $\mathbf{c}_{p}$ is a constant vector, to be determined by the eigenvalue problem that results from the plasma–vacuum matching.

In the second step of the matching procedure, we consider the matching at the plasma–vacuum interface. Since $\nabla \cdot \delta\vec{B} = 0$, the normal component of the magnetic field $\delta\vec{B}$ should be continuous across this interface.

With the use of this condition, the $\mathbf{c}_v$ in Eq. (22) can be related to $\mathbf{c}_p$ in Eq. (28). This matching can be shown to yield

$$\mathbf{u}_{v2}(\psi_a) = \mathscr{U}_{v2}^{M \times M}(\psi_a)\mathbf{c}_v = -i\left[\chi' \mathscr{T} \mathscr{K}_{\parallel}\right]_{\psi=\psi_a}\mathbf{c}_p. \tag{29}$$

Here, Eq. (27) has been used. Having different vacuum and plasma coordinate systems provides flexibility. The transform matrix between the two poloidal coordinates (θ_v for vacuum) and (θ_p for plasma) is defined as follows:

$$\mathscr{T}_{m_v m_p} = \frac{1}{2\pi} \int_{-\pi}^{\pi} d\theta_p e^{-im_v \theta_v} e^{im_p' \theta_p}.$$

When non-PEST coordinates (e.g., Hamada coordinates) are used in the plasma region, the theta-dependent part of the generalized toroidal angle should also be included in this transformation. One can solve Eq. (29) to obtain

$$\mathbf{c}_v = -i\left[\chi' \mathscr{U}_{v2}^{-1} \mathscr{T} \mathscr{K}_{\parallel}\right]_{\psi=\psi_a}\mathbf{c}_p. \tag{30}$$
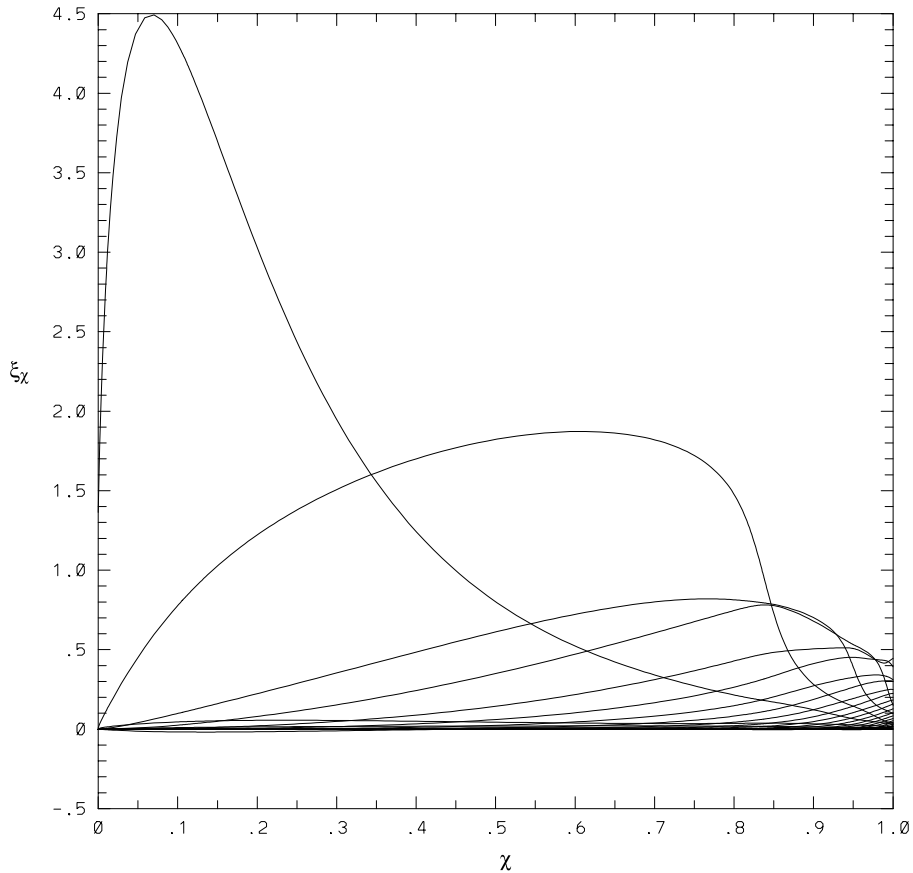
Fig. 5. $n = 1$ modes computed by AEGIS in the configuration described in Fig. 1. The poloidal magnetic flux χ is used as the horizontal coordinate and the Fourier components of $\xi_\chi = \vec{\xi} \cdot \nabla\chi$ as the vertical coordinate.

Using $\mathbf{c}_v$ one can obtain

$$\mathbf{u}_{v1}(\psi_a) = \mathscr{U}_{v1}(\psi_a)\mathbf{c}_v = -\mathrm{i}\big[\mathscr{U}_{v1}\mathscr{U}_{v2}^{-1}\mathscr{T}\mathscr{K}_{\parallel}\big]_{\psi=\psi_a}\mathbf{c}_p. \tag{31}$$

For simplicity, the superscript indicating the rank of the respective matrix will henceforth be dropped.

Inserting Eqs. (29) and (31) into the vacuum energy integral in Eq. (19) and inserting Eqs. (27) and (28) into the potential and kinetic energies of the plasma in Eq. (12), one finds that the total system energy is reduced to

$$2\mu_0\big(\delta W_p + \delta W_k + \delta W_v\big) = \mathbf{c}_p^{\dagger}\Big[\mathscr{U}_{p2} - \chi'^2\mathscr{K}_{\parallel}\mathscr{T}^{\dagger}\mathscr{U}_{v2}^{-1\dagger}\mathscr{U}_{v1}^{\dagger}\mathscr{T}\mathscr{K}_{\parallel}\Big]_{\psi=\psi_a}\mathbf{c}_p. \tag{32}$$

This total energy can be further minimized with respect to $\mathbf{c}_p^{\dagger}$. Stability is then determined by the condition of whether the minimized energy is positive or negative. To evaluate this condition, an artificial kinetic energy $\delta W_a = \Omega^2\int\mathrm{d}\psi\,\mathbf{c}^{\dagger}\mathbf{c}$ is introduced in the minimization, as is also done in the DCON and ELITE codes. This yields the final eigenmode equation:

$$\Big[\mathscr{U}_{p2} - \chi'^2\mathscr{K}_{\parallel}\mathscr{T}^{\dagger}\mathscr{U}_{v2}^{-1\dagger}\mathscr{U}_{v1}^{\dagger}\mathscr{T}\mathscr{K}_{\parallel}\Big]_{\psi=\psi_a}\mathbf{c}_p = \Omega^2\mathbf{c}_p. \tag{33}$$

The solution of this equation constitutes a linear Hermitian eigenvalue problem. The sign of the eigenvalue Ω^2 indicates stability: If the eigenvalue is positive ($\Omega^2 \geqslant 0$), the system is stable; otherwise it is unstable. From the eigenvector, the eigenmode in the plasma region can be determined from Eq. (28) and that in the vacuum region from (22) (together with Eq. (30)). Note that the eigenvalue $\Omega^2(\lambda)$ is a function of the actual growth rate γ. The true eigenmode is the one that satisfies Eq. (33) with $\Omega^2(\lambda) = 0$. The condition $\Omega^2(\lambda) = 0$ is a dispersion relation. A Nyquist diagram approach can be used to determine the unstable roots. Since the system is Hermitian, there are only real values of $\Omega^2(\lambda)$. Therefore, examining the change in the sign of $\Omega^2(\lambda)$ is sufficient to determine the stability of a system. When non-ideal MHD effects are taken into account, the problem becomes non-Hermitian and a full Nyquist diagram analysis would be required.
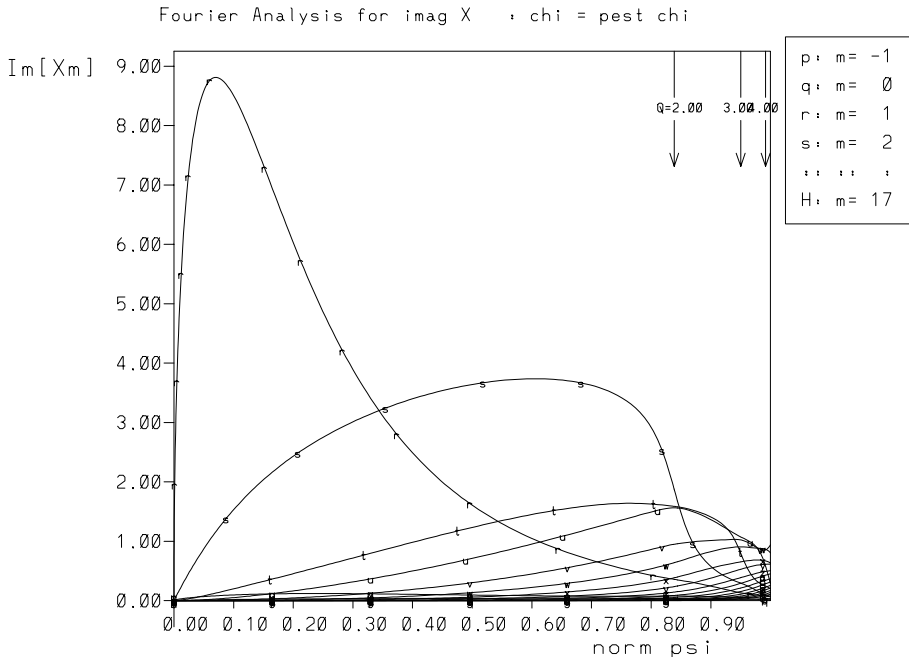

Fig. 6. The same modes as Fig. 5 computed by GATO.

4. Numerical results and benchmark studies

The numerical scheme described in the preceding section has been implemented in the AEGIS code with Fortran 90/95 on the Seaborg IBM SP supercomputer at the National Energy Research Scientific Computing Center. Both NAG and IMSL mathematical libraries were employed in the coding. The results were benchmarked with the GATO code, and good agreement was found in all respects, such as the stability beta limit, the growth rate, the mode shape, the critical wall position, etc.

Figs. 5 and 6 compare the $n = 1$ modes computed by the AEGIS and GATO codes, respectively, for the equilibrium described in Fig. 1. The $n = 3$ modes are compared in Figs. 7 and 8. Due to its adaptive nature, the AEGIS code has better resolution than GATO at the mode resonance surfaces. The consequence is that AEGIS can calculate MHD modes that have small growth rate. Using various equilibria, we found that the growth rate for modes that can be computed with AEGIS can be one or two orders of magnitude smaller than for modes computed with GATO.

In a non-adaptive code that calculates MHD modes, the grid density must be increased near the resonance surfaces. Moreover, for modes with high mode numbers, there are many mode resonance surfaces. The number of radial grid points, then, must be dramatically increased in order to attain the required resolution in the vicinity of the resonance surfaces. Consequently the size of the eigenmatrix in a non-adaptive
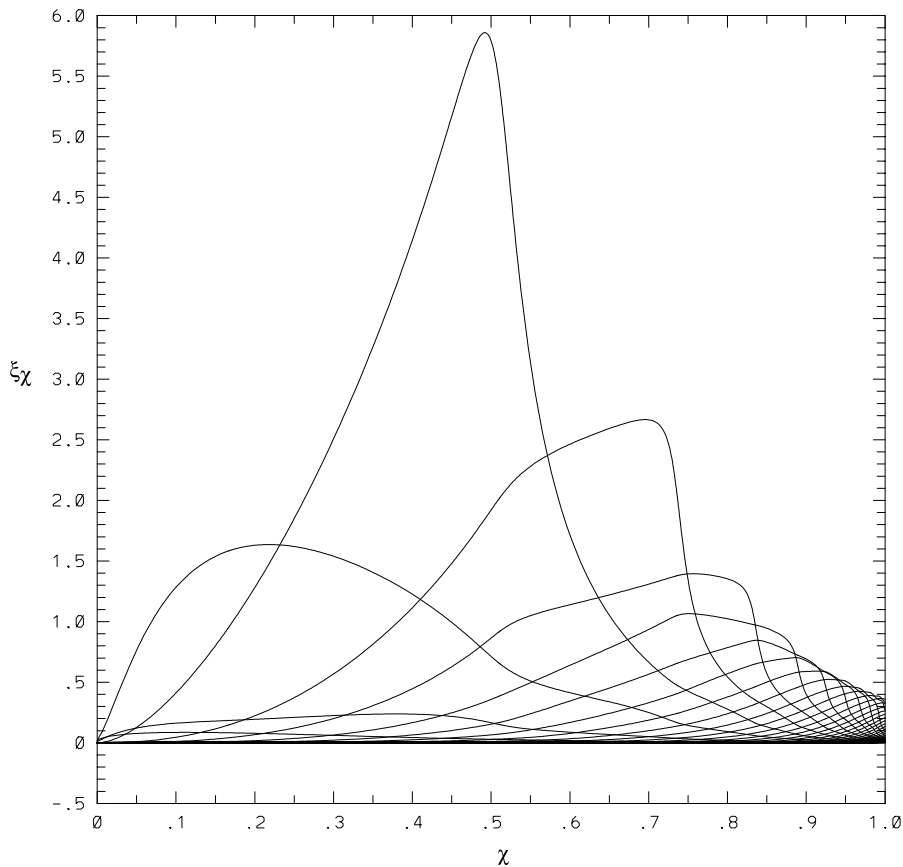

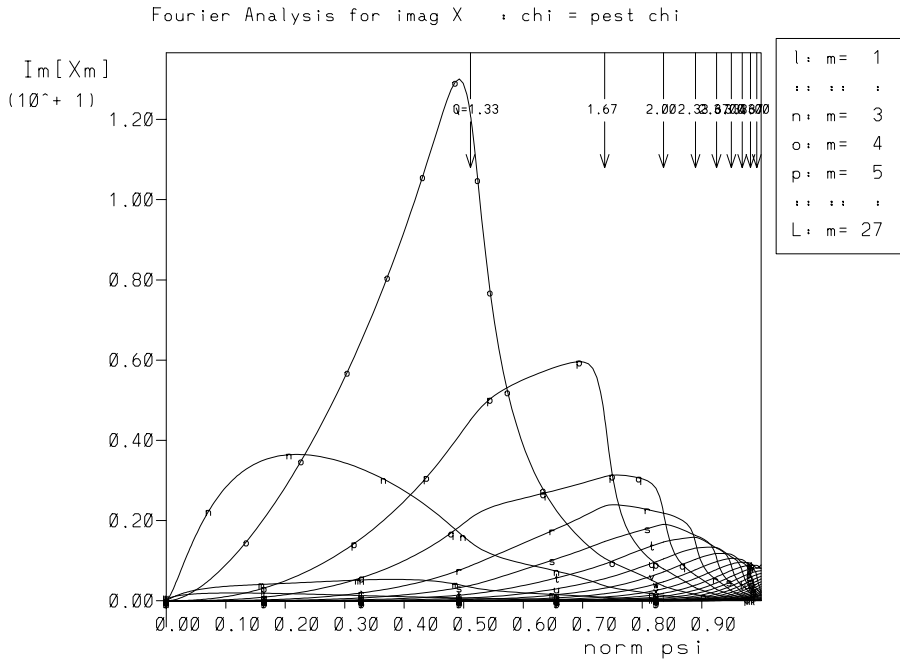Fig. 7. $n = 3$ modes computed by AEGIS in the configuration described in Fig. 1.

Fig. 8. The same modes as Fig. 7 computed by GATO.

code increases enormously (by a factor that is approximately given by the number of resonance surfaces multiplied by the number of additional grid points needed for good resolution near resonance surfaces). However, with the independent-solution shooting method in the AEGIS code, the matrix size increases only by a factor given by the number of resonance surfaces [see Eq. (24)]. Thus, the AEGIS code can be used to compute high-mode-number modes within a comfortably short computing time. The $n = 10$ modes computed with AEGIS are shown in Fig. 9. This feature of the AEGIS code is inherited from a similar feature in the ELITE code [13].

5. Conclusions and discussion

The development of the linear ideal-MHD adaptive shooting code AEGIS has been described. Its numerical scheme can be summarized as follows. Fourier decomposition is used in the poloidal direction. In the radial direction, the modes are decomposed into a linear combination of the complete set of independent solutions of the Euler–Lagrange equations. The adaptive shooting method is used to obtain these independent solutions. The shooting in the plasma region is divided into shootings in multiple subregions, with the solutions in the subregions matched to each other. This procedure overcomes the numerical difficulty associated with the stiff nature of the independent solutions near the singular surfaces and the magnetic axis. A similar scheme is also used for the vacuum region. Shooting in the vacuum region is much simpler than that in the plasma region, since there are no resonance surfaces in the vacuum. The eigenvalue equation is formulated by the matching of the plasma and vacuum solutions. AEGIS contains a built-in interface with the numerical equilibrium, which is computed, for example, by the TOQ code, after which regridding is performed and the numerical equilibrium is checked with the Glad-Shafronov equation.
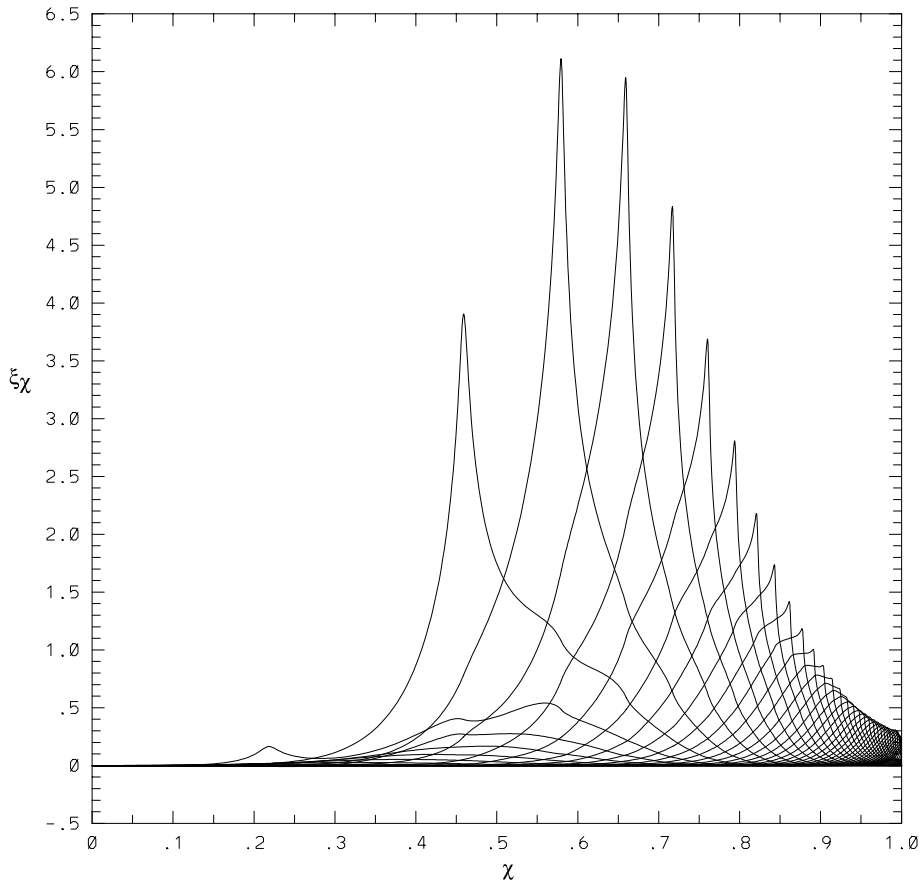
Fig. 9. $n = 10$ modes computed by AEGIS in the configuration described in Fig. 1.

The AEGIS code has been benchmarked with the GATO code for various equilibria with different values for the aspect ratio, elongation, triangularity, etc. The results for the stability beta limit, the growth rate, the mode shape, the critical wall position, etc., were found to be in very good agreement. A comparison with analytical results in the cylindrical geometry limit has been also performed and good agreement was again obtained.

In contrast to non-adaptive codes such as PEST and GATO (as well as ELITE), the adaptive shooting method in AEGIS provides higher resolution near the mode singular surfaces. This allows AEGIS to be able to compute the MHD modes with growth rates that are one or two orders of magnitude smaller than those for the MHD modes that can be computed with non-adaptive codes. The adaptive feature of AEGIS is particularly useful for studying equilibria – such as equilibria with thin transport barriers or equilibria for highly elongated tokamaks – for which it is difficult to achieve numerical convergence in grid codes.

Another advantage is that AEGIS can compute modes with both low and medium-to-high mode numbers. Let us compare AEGIS and ELITE for high-n mode computations. As the basic set of equations for stability computation, AEGIS uses the full incompressible MHD equations, whereas ELITE uses the reduced MHD equations for the ballooning mode stream function in the high-n ordering. AEGIS is a full-radius MHD code and can investigate both core and edge modes, whereas ELITE is used to study only edge localized modes. In most studies of the stability of MHD modes in tokamaks, two-dimensional codes

are used to study the low-mode-number modes (up to about $n = 5$), while an one-dimensional ballooning code (together with the Mercier criterion) is used to assess the high-n modes in the core of the plasma and the ELITE code can be used to investigate the high-n modes at the plasma edge. In contrast, with AEGIS the modes with intermediate mode numbers, between $n = 5$ and $n = 10$, can be investigated as well. In studies of high-n modes, AEGIS can address the coupling between the core and edge high-n modes.

It is also of interest to compare AEGIS with DCON. Both DCON and AEGIS are based on decomposing the general solution into a linear summation of the independent solutions of the Euler–Lagrange equations to facilitate the radially adaptive shooting. The difficulty of this approach lies in how to compute the independent solutions accurately, since the large solutions of the Euler–Lagrange equations are overwhelmingly dominant over the small solutions, especially near the singular surfaces and at the magnetic axis. A brute force numerical shooting treatment fails in general to get the independent solutions over the entire plasma region. The small solutions are often submerged in the numerical noise of the large solutions. To overcome this difficulty, the DCON code uses the Gaussian elimination technique to remove the large solution, while the AEGIS code employs the piece-wise multiple-region shooting and matching technique to obtain both the large and small solutions. The DCON code uses its numerical scheme to calculate MHD marginal stability. By contrast, the AEGIS numerical scheme solves the finite-frequency problem. An extrapolation is required with AEGIS to obtain the MHD marginal stability boundary. The ultimate objective of the AEGIS code is to be able to treat rotational and kinetic effects; the generalization of the code for this objective is currently under way. In order to treat the non-ideal MHD case, the role of finite frequency or growth rate needs to be addressed. The AEGIS multiple-region-matching numerical scheme can be extended directly to treat the non-ideal MHD case.

Acknowledgments

References

[1] R.C. Grimm, J.M. Greene, J.L. JohnsonMethods of Computational Physics, vol. 9, Academic Press, New York, London, 1976, pp. 253–280.

[2] M.S. Chance, J.M. Greene, R.C. Grimm, J.L. Johnson, J. Manickam, W. Kerner, D. Berger, L.C. Bernard, R. Gruber, F.J. Troyon, Comparative numerical studies of ideal magnetohydrodynamic instabilities, J. Comput. Phys. 28 (1978) 1–13.

[3] R. Gruber, F. Troyon, D. Berger, L.C. Bernard, S. Roussert, R. Schreiber, W. Kerner, W. Schneider, K.V. Roberts, ERATO stability code, Comput. Phys. Commun. 22 (1981) 323–377.

[4] R. Gruber, F. Troyon, S. Roussert, W. Kerner, L.C. Bernard, Transform of ERATO into a δW code, Comput. Phys. Commun. 22 (1981) 383–387.

[5] L.C. Bernard, F.J. Helton, R.W. Moore, GATO: An MHD stability code for axisymmetric plasmas with internal separatrices, Comput. Phys. Commun. 24 (1981) 377–380.

[6] R.C. Grimm, R.L. Dewar, J. Manickam, Ideal MHD stability calculations in axisymmetric toroidal coordinate systems, J. Comput. Phys. 49 (1983) 94–117.

[7] A.H. Glasser, The direct criterion of Newcomb for the stability of an axisymmetric toroidal plasma, Los Alamos Report LA-UR-95-528, 1997.

[8] C.Z. Cheng, M.S. Chance, NOVA: A nonvariational code for solving the MHD stability of axisymmetric toroidal plasmas, J. Comput. Phys. 71 (1987) 124–146.

[9] A. Bondeson, G. Vlad, H. Luetjens, Resistive toroidal stability of internal kink modes in circular and shaped tokamaks, Phys. Fluids B 4 (1992) 1889–1900.

[10] L. Degtyarev, A. Martynov, S. Medvedev, F. Troyon, L. Villard, R. Gruber, The KINX ideal MHD stability code for axisymmetric plasmas with separatrix, Comput. Phys. Commun. 103 (1997) 10–27.

[11] A.B. Mikhailovskii, G.T.A. Huysmans, S.E. Sharapov, W. Kerner, Optimization of computational MHD normal mode analysis for tokamaks, Plasma Phys. Rep. 23 (1997) 844–857.

[12] W.A. Newcomb, Hydromagnetic stability of a diffuse linear pinch, Ann. Phys. (N.Y.) 10 (1960) 232–267.

[13] H.R. Wilson, P.B. Snyder, G.T.A. Huysmans, R.L. Miller, Numerical studies of edge localized instabilities in tokamaks, Phys. Plasmas 9 (2002) 1277–1286.

[14] P.B. Snyder, H.R. Wilson, J.R. Ferron, L.L. Lao, A.W. Leonard, T.H. Osborne, A.D. Turnbull, D. Mossessian, M. Murakami, X.Q. Xu, Edge localized modes and the pedestal: a model based on coupled peeling ballooning modes, Phys. Plasmas 9 (2002) 2037–2043.

[15] H.R. Wilson, R.L. Miller, Access to second stability region for coupled peeling–ballooning modes in tokamaks, Phys. Plasmas 6 (1999) 873–876.

[16] R.L. Miller, J.W. Van Dam, Hot particle stabilization of ballooning modes in tokamaks, Nucl. Fusion 27 (1987) 2101–2112.

[17] S. Hamada, Hydromagnetic equilibria and their proper coordinates, Nucl. Fusion 2 (1962) 23–37.

[18] M.S. Chance, Vacuum calculations in azimuthally symmetric geometry, Phys. Plasmas 4 (1997) 2161–2180.

[19] R. Gruber, J. Rappaz, Finite Element Methods in Linear Ideal Magnetohydrodynamics, Springer, Berlin, 1985.